ACS APPLIED MATERIALS & INTERFACES

Research Article

www.acsami.org

Superhydrophobic Hierarchically Assembled Films of Diblock Copolymer Hollow Nanospheres and Nanotubes

Guping He,[†] Jiwen Hu,*[,†] Guojun Liu,*[,†,‡] Yinhui Li,[†] Ganwei Zhang,[†] Feng Liu,[†] Jianpin Sun,[†] Hailiang Zou,[†] Yuanyuan Tu, and Dingshu Xiao[†]

[†]Guangzhou Institute of Chemistry, Chinese Academy of Sciences, Guangzhou, P.R. China, 510650

[‡]Department of Chemistry, Queen's University, 90 Bader Lane, Kingston, Ontario, Canada K7L 3N6

S *Supporting Information*

ABSTRACT: Reported are the formation of rough particulate films from cross-linked diblock copolymer vesicles and nanotubes and the wetting properties of the resultant films. The diblock copolymers used were $F_{66}M_{200}$ and $F_{95}A_{135}$, where the subscripts denote the repeat unit numbers, whereas M, A, and F denote poly(2-cinnamoyloxyethyl methacrylate), poly(2-cinnamoyloxyethyl acrylate), and poly(2,2,2-trifluoroethyl methacrylate), respectively. The precursory polymers to $F_{66}M_{200}$ and $F_{95}A_{135}$ were prepared by atom transfer radical polymerization. In 2,2,2-trifluoroethyl methacrylate (FEMA), a selective solvent for F, vesicles and tubular micelles were prepared from $F_{66}M_{200}$ and $F_{95}A_{135}$, respectively. Photo-cross-linking the M and A blocks of these aggregates yielded hollow nanospheres and nanotubes bearing F coronal chains. These particles were dispersed into CH_2Cl_2/methanol, where CH_2Cl_2 was a good solvent for both blocks and methanol was a poor solvent for F. Casting CH_2Cl_2/methanol dispersions of these particles yielded films consisting of hierarchically assembled diblock copolymer nanoparticles. For example, the hollow nanospheres fused into microspheres bearing nanobumps after being cast from CH_2Cl_2/methanol at methanol volume fractions of 30 and 50%. The roughness of these films increased as the methanol volume fraction increased. The films that were cast at high methanol contents were superhydrophobic, possessing water contact angles of ~160° and water sliding angles of ~3°.

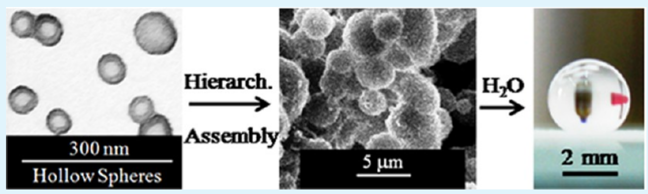

KEYWORDS: *block copolymers, self-assembly, micellization, hierarchical assembly, superhydrophobicity*

1. INTRODUCTION

On a superhydrophobic surface,[1] water droplets have contact angles larger than 150°. Also, the difference between the advancing and receding contact angles or contact angle hysteresis should be small, so that the droplets readily roll off of the surface. Examples of superhydrophobic surfaces from nature include lotus leaves[2] and water-strider legs.[3]

Many applications are anticipated for superhydrophobic surfaces. For example, skyscrapers with superhydrophobic walls would require minimal cleaning.[4] Power cables that are covered by a superhydrophobic coating would be protected against ice accumulation and damage from ice storms.[5] Also, a superhydrophobic coating on metal surfaces should help reduce metal rusting and corrosion.[6a−d]

Since the surface tension of water is high at 72.8 mN/m at 20 °C, many organic compounds or polymers possessing surface tensions of ~30 mN/m or lower may be used to create superhydrophobic coatings. The key to superhydrophobicity in these cases is to have a coating that bears roughness on both the micrometer and nanometer scales.[7−9] Many interesting and sometimes exotic methods have been developed over the past decade for creating rough surfaces. These have included lithography,[10,11] deposition of premade particles,[12] generation of surface bumps via surface crystal formation or polymer phase separation,[13] surface initiated whisker or fiber formation,[14,15] and polymer fiber formation due to solvent evaporation from a columnar polymer solution.[16] Other methods have utilized superhydrophobic films from cross-linked fluorinated microspheres[17] or electrospun fibers,[18] among other examples. Of these different methods, deposition of premade particles seems to be the most straightforward.

When premade particles are deposited, these particles are normally imparted with fluorinated surfaces to take advantage of the low surface tension of fluorinated polymers. Many methods have been reported for the preparation of fluorinated particles.[19−22] For example, core−shell (CS) particles with a fluorinated shell have been prepared via seeded emulsion polymerization using nanosized silica particles as the seeds.[23] The reaction between calcium chloride and sodium carbonate in the presence of fluoroalkyl end-capped acrylic acid allowed the preparation of fluorinated calcium carbonate particles.[24] Silica, alumina, and polymer particles were fluorinated via surface functionalization using perfluoroalkyl chlorosilane,[25] perfluoroalkyl acid chloride,[22] and a diblock copolymer[21] bearing a fluorinated block. Furthermore, the reduction of gold ions by poly(methylhydrosiloxane) in the presence of

Received: July 8, 2012
Accepted: March 12, 2013
Published: March 12, 2013

fluoroalkyl end-capped co-oligomeric nanoparticles yielded a novel class of fluorinated co-oligomeric nanocomposite-encapsulated gold nanoparticles.[26]

Block copolymers undergo self-assembly in block-selective solvents to form micelles of various shapes, ranging from spheres, to cylinders, to vesicles.[27−30] The smallest dimension of these particles is typically on the scale of tens of nanometers. They are stabilized in the block-selective solvents because of their soluble coronal chains. The insoluble block in the case of a diblock copolymer makes up the core of the spherical and cylindrical micelles and the wall of the vesicles. Through the choice of an appropriate block copolymer and using the right chemistry, the insoluble domains of these micelles can be easily cross-linked to help lock in the shape of these aggregates and thus yield "permanent" nanoparticles.[31−34] We imagined that these particles might be cast from solutions to yield rough films. If the coronal block was properly chosen, superhydrophobic films might be obtained. Reported in this paper are our preliminary efforts in this endeavor and the materialization of these ideas.

The polymers used in this study were poly(2,2,2-trifluoroethyl methacrylate)-*block*-poly(2-cinnamoyloxyethyl methacrylate) (PFEMA-*b*-PCEMA, also abbreviated as FM) and PFEMA-*b*-PCEA (abbreviated as FA). Here PCEA denoted poly(2-cinnamoyloxyethyl acrylate). The structure of FM is depicted in Scheme 1.

Scheme 1. Chemical Structure of PFEMA-*b*-PCEMA (FM)

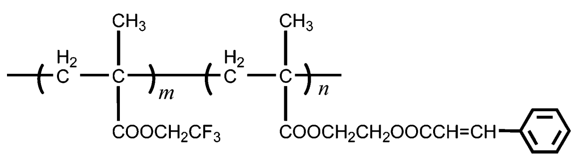

The F block was chosen mainly as an inexpensive model fluorinated block. The C block was targeted for its demonstrated ability to undergo photo-cross-linking without additives and its use in locking various block copolymer micelles and block-segregated solids to yield structures such as nanospheres,[31] hollow nanospheres,[35] nanofibers,[32] nanotubes, thin films containing nanochannels,[36] and cross-linked diblock copolymer brushes (monolayers).[37] These copolymers were assembled into vesicles and tubular micelles and subsequently photo-cross-linked. The morphologies of films cast from these particle dispersions and the water wetting properties of these particulate films were investigated in this report.

Although we are unaware of reports on superhydrophobic films made of cross-linked diblock copolymer micelles or vesicles, diblock copolymer spherical micelles have been used by Xu and co-workers[38a,b] and other researchers[39a−d] to prepare superhydrophobic films. Our system differs from the systems studied by prior researchers in the polymers and chemistry used. Also, our particles were cross-linked and possessed different shapes. Rather than being spherical micelles, they possessed vesicular and tubular structures. The study of structurally locked particles of various shapes was expected to shed light on how the shape of the particles was to affect their hierarchical assembly and the wetting properties of the resultant particulate films.

2. EXPERIMENTAL SECTION

2.1. Materials. 2,2,2-Trifluoroethyl methacrylate (FEMA) was a product of Harbin Xuefugui Chemical Co., Ltd. (China). After it was washed with a 2 wt % NaOH aqueous solution and doubly distilled water, the organic layer was dried over anhydrous $MgSO_4$. Subsequently, $MgSO_4$ r was emoved via filtration and FEMA was distilled under reduced pressure. Cuprous bromide (CuBr, Fluka, 98+ %) was stirred in acetic acid at 80 °C for 8 h, washed with methanol 10 times, and dried under vacuum at room temperature overnight.[40] Cuprous chloride (CuCl, Aldrich, 99%) was purified analogously. *N,N,N,N,N*-Pentamethyldiethylenetriamine (PMDETA) (99%) and 2,2-bipyridine (bpy) (99%) were used as received from Aldrich. Cyclohexanone (99.8%, Tianjin Baishi Chemical Co.) was initially decolored by active charcoal, and then stirred overnight with calcium hydroxide (Aldrich, 99%) before vacuum distillation. 2-Hydroxyethyl methylacrylate (HEMA, 98%, Sigma Aldrich), 100 mL, was mixed with 300 mL of distilled water and extracted eight times with hexanes at 50 mL per extraction. Lastly, the monomer was salted out through the addition of ∼100 g of NaCl. The organic phase was dried over $MgSO_4$ and then vacuum-distilled.[41] Cinnamoyl chloride (98%, predominantly trans) was purchased from Aldrich and used without further treatment. Tetrahydrofuran (THF), diethyl ether, and hexane were all of analytical grade and distilled over sodium prior to use. Acetonitrile, dichloromethane, and methanol were distilled before use. Methoxyethyl 2-bromoisobutyrate (In−Br) was prepared following a procedure that we have described in a previous report.[42]

2.2. Macroinitiator PFEMA-Br (F−Br). FEMA ATRP was performed in a homemade flask that consisted of two 25 mL round-bottomed flasks joined via a fused glass tube with an internal diameter of 0.8 cm. To prepare F−Br with 66 units, the solvent cyclohexanone (12.9 g), FEMA (8.0323 g, 47.8 mmol), In−Br (107.7 mg, 0.478 mmol), and bpy (147.2 mg, 0.956 mmol) were added into one of the twin flasks. Meanwhile, CuBr (68.8 mg, 0.478 mmol) was loaded into the other flask. The liquid mixture in the former flask was then subjected to three freeze−pump−thaw cycles for oxygen removal before it was transferred into the latter flask containing CuBr to yield a solution bearing a brownish red color. The flask was immersed into an oil bath that had been preheated at 80 °C, and the mixture was magnetically stirred. Over 1 h, the brownish red solution turned light green and then dark green, and the solution viscosity was seen to increase. Subsequently, the flask was immersed into liquid nitrogen and the vacuum valve was opened to allow the entry of air. The introduced air immediately turned the reaction mixture from green to blue, suggesting that Cu(I) had become oxidized. The blue reaction mixture was diluted with 5 mL of THF before it was eluted with THF through a neutral alumina column to remove the copper complex. The filtrate was concentrated to ∼5 mL by rotary evaporation and added into 100 mL of hexane to precipitate F−Br. The crude product was redissolved into 5 mL of THF and precipitated from 100 mL of hexane. This process was repeated another time. The final precipitate was vacuum-dried overnight to generate 6.2 g of the F−Br macroinitiator as a white powder. ^1H NMR ($CDCl_3$): δ 4.32 (br s, $-CH_2CF_3$); δ 3.35 (br s, -OCH_3); δ 1.75−2.05 (m, $-CH_2$); δ 0.75−1.35 (m, $-CH_3$). To determine the corrected degree of polymerization (DP) value, we used end-group analysis to evaluate the DP of the first F−Br block from ^1H NMR by taking advantage of the end group provided by the initiator, In−Br.[42] A comparison between the integrals of the small peak at 3.35 ppm corresponding to the -OCH_3 protons of the initiator In−Br and of the peak at 4.32 ppm allowed the determination of the DP for F−Br, which was found to be 66. Another sample of F−Br with 95 repeat units was also prepared and characterized analogously.

2.3. PFEMA-*b*-PHEMA and PFEMA-*b*-PHEA. The copolymers PFEMA-*b*-PHEMA and PFEMA-*b*-PHEA were synthesized as precursors to FM and FA. To prepare PFEMA-*b*-PHEMA, acetonitrile (2.7618 g), HEMA (2.7568 g, 22.1 mmol), bpy (24.7 mg, 0.158 mmol) were added into one of the flasks within the twin flask system. Meanwhile, F_{66}−Br (0.5050 g, 0.0455 mmol) and CuCl (7.9 mg, 0.079 mmol) were added to the other flask. The liquid reactants were

Scheme 2. Synthetic Pathway for Preparing $F_{66}M_{200}$ from the Macroinitiator F_{66}−Br

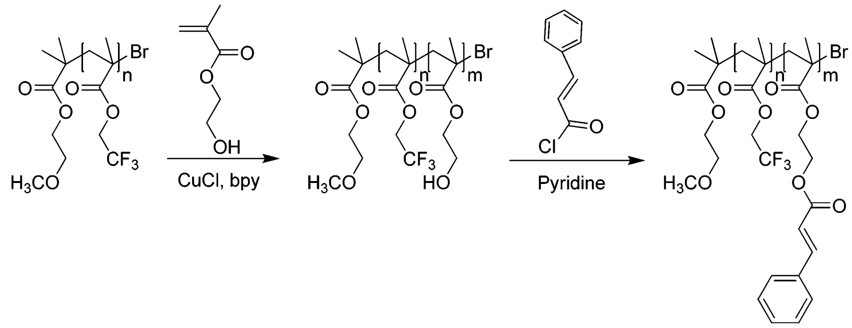

subjected to three freeze−pump−thaw cycles before they were transferred to the flask containing the F_{66}−Br and CuCl solids. This brownish red solution was stirred to dissolve the solid and then placed into an oil bath that had been preheated to 40 °C. After 8 h, the reaction was stopped by freezing the mixture in liquid nitrogen and exposing it to air. The mixture was added into 200 mL of distilled water to precipitate the polymer. The precipitate was washed thrice with 100 mL of hexane (3 × 100 mL) before it was vacuum-dried, yielding 2.35 g of product as a white powder. ^{1}H NMR analysis in DMSO-d_6: δ 4.62 (br s, 2nH, $-CH_2CF_3$); δ 3.85 (br s, 2mH $-COOCH_2-$ in the PHEMA chains); δ 3.55 (br s, 2mH, $-CH_2OH$); δ 4.8 (br s, mH, −OH). The repeat unit number ratio between the two blocks was determined from the integration ratios of the peaks at 4.62 ppm corresponding to $-CH_2CF_3$ protons and at 3.85 ppm corresponding to $-COOCH_2-$ protons in the F and PHEMA chains, respectively.[25] PFEMA-*b*-PHEA was prepared and characterized analogously.

2.4. FA and FM. Cinnamation was performed according to a literature method.[25] Cinnamoyl chloride, at 1.8 mol equiv relative to the hydroxyl groups of PFEMA-*b*-PHEMA, was stirred overnight in dry pyridine. The mixture was filtered to remove the pyridinium salt that had formed, and was subsequently added into a 10-fold volume excess of ethanol. The precipitate was rinsed thrice with ethanol before it was dried under a vacuum to yield a white powder. Full cinnamation was confirmed by ^{1}H NMR spectroscopy.

2.5. Micelles or Vesicles Preparation and Cross-linking. FA or FM (250 mg) was stirred with 25 mL of FEMA for 7 d to yield a micellar dispersion. The micellar dispersions were subsequently photolyzed in a 25 mL quartz cell for 15 h using light from a 55 W Philips-TUV lamp. The degree of cross-linking was determined from the absorbance decrease at 273 nm,[31] and was adjusted to between 30 and 40%.

After photolysis, the solutions were concentrated to ∼10 mL and added into ∼100 mL of hexane. The precipitate was rinsed thrice with hexane at 5 mL each time and subsequently vacuum-dried to yield cross-linked particles in an essentially quantitative yield.

2.6. Particulate Films. Particulate films were cast from CH_2Cl_2/methanol dispersions of the cross-linked micelles or vesicles with methanol volume fractions f_{MeOH} ranging between 0 and 50%. The dispersions were prepared by initially dissolving the nanoparticles in CH_2Cl_2 at 5 mg/mL. Methanol was then added to the desired f_{MeOH}. Evidently, the most dilute nanoparticle dispersion used had a concentration of 2.5 mg/mL at f_{MeOH} = 50%. A particulate film was prepared by dispensing a few droplets of a dispersion onto a clean glass slide and evaporating the solvent at room temperature.

2.7. Polymer Characterization. ^{1}H NMR spectra were recorded in deuterated chloroform on a Bruker DMX-400 spectrometer equipped with a Varian probe. Size exclusion chromatography (SEC) was performed at 35 °C using a Waters 1515 series system equipped with styragel HR4 and HR3 columns and a Waters 2414 refractive index (RI) detector. The system was calibrated with narrowly dispersed polystyrene standards and the mobile phase used was HPLC grade DMF flowing at 0.60 mL/min.

2.8. TEM, SEM, and AFM. Transmission electron microscopy (TEM) measurements were performed using a JEM-100CXIImicroscope at an accelerating voltage of 80 kV. Micellar solutions were aerosprayed using a home-built device[43] onto nitrocellulose-covered copper grids. After the samples were dried at room temperature for 1 h, they were subsequently stained with RuO_4 vapor for 2.5 h before observation by TEM.

Scanning electron microscopy (SEM) images of particulate films were obtained with a Hitachi S-4800 instrument and the field-emission electron microscopy analysis was performed using a JSM-5910 instrument. The films were prepared at room temperature under an atmosphere with 60−80% humidity by dropping a ∼1 mg/mL particulate dispersion onto a 5 × 5 mm^2 glass plate. SEM images were obtained after the films were coated with a thin layer of gold.

For atomic force microscopy (AFM) measurements, the aggregate solutions were directly aero-sprayed onto freshly cleaved mica surfaces. The images were obtained using a Bruker Multimode 8 AFM equipped with a Nanoscope Vcontroller operating in the tapping mode. The tips used were of model RTESP of the Bruker NanoProbeTM type and a radius of curvature typically less than 12 nm.

The average sizes of the aggregates assembled from copolymer, cross-linked hollow spheres or nanotubes were determined from TEM, SEM, or AFM images. In particular, these calculations were based on a few micrographs which displayed a total population (n) of more than 100 individual aggregates. The average size ($\overline{X}$) and standard deviation (sd) were defined as $\overline{X} = (\Sigma_{i=1}{}^{n}X_i)/n$ and sd = $((\Sigma_{i=1}{}^{n}(X_i - X)^2/(n - 1))^{(1)/(2)})$, respectively.

2.9. Contact Angle Measurements. Measurements were performed using a Dataphysics OCA40 plus contact angle system with contact angles attained by the pendant drop method.[42] Films for contact angle measurements were prepared at room temperature under an atmospheric humidity of 60−80% by dropping and evaporating a few droplets of a ∼1 mg/mL particle dispersion onto glass slides, which were prerinsed sequentially with methanol, acetone, and deionized water. Water droplets (5 μL in volume) were dispensed via a microsyringe and the images were recorded using a CCD camera ∼1 min after the droplets were dispensed. The contact angles of each sample were reported as the average of measurements recorded at ∼10 positions on the surface of a given film.

2.10. Sliding Angle Measurements. The sliding angle was evaluated by tilting the sample stage from 0° to higher angles and then placing an 8 μL water droplet on the sample surface using a pipet. When the droplet rolled off the surface, the angle of the sample stage was considered as the sliding angle. For each sample, the measurements were performed at least 5 times, and the reported values were the averages of these measurements.

3. RESULTS AND DISCUSSION

3.1. Polymer Synthesis and Characterization. Precursors to $F_{66}M_{200}$ and $F_{95}A_{135}$ were prepared via atom transfer radical polymerization (ATRP). The synthetic route for preparing $F_{66}M_{200}$ from the macroinitiator F_{66}−Br is illustrated in Scheme 2. $F_{95}A_{135}$ was prepared using an analogous route. The ^{1}H NMR spectra with peak assignments for $F_{66}M_{200}$,

$F_{95}A_{135}$ and their precursors are included in Figures S1 and S2 in the Supporting Information.

The synthesis of macroinitiator F−Br and the ATRP kinetics of FEMA have been recently reported and will thus not be discussed further.[42] The two macroinitiators used were carefully characterized by ^{1}H NMR spectroscopy as described in the Experimental Section and were shown to have the repeat unit numbers of 66 and 95. The size exclusion chromatography (SEC) polydispersity index (M_w/M_n) based on PS standards were 1.28 and 1.25, respectively, for the two macroinitiators.

HEMA or HEA was polymerized in acetonitrile at 40 °C using CuCl and 2,2-bipyridine as the catalytic system. The resultant diblock copolymer, either PFEMA-*b*-PHEMA or PFEMA-*b*-PHEA, was cinnamated by reacting the hydroxyl groups of PHEMA or PHEA with cinnamoyl chloride.[31]

Table 1 lists the characteristics of the macroinitiators F−Br and the diblock copolymers. While ^{1}H NMR analysis was performed in $CDCl_3$, SEC was performed using DMF as the eluant and polystyrene as the calibration standards. The diblock copolymers used had rather low polydispersity indices and F weight fractions f_F of 18% and 46% for $F_{66}M_{200}$ and $F_{95}A_{135}$, respectively.

Table 1. Molecular Characteristics of the F−Br Macroinitiators and Diblock Copolymers

	macroinitiator		diblock copolymer			
sample	NMR n	SEC M_w/M_n	NMR n/m	m	f_F (%)	SEC M_w/M_n
$F_{66}M_{200}$	66	1.28	1.00/3.0	200	18	1.26
$F_{95}A_{135}$	95	1.25	1.00/1.42	135	33	1.21

3.2. Micelle or Vesicle Preparation and Cross-linking.

Micelles or vesicles were prepared by directly dispersing $F_{66}M_{200}$ and $F_{95}A_{135}$ in FEMA. To cross-link the assembled aggregates, we irradiated these micellar solutions with a UV lamp under vigorous stirring for 15 h. The double bond conversions were determined from decreases in the UV absorbance at 273 nm before and after photolysis of the aggregates.

The aggregates were aero-sprayed both before and after cross-linking treatment using a home-built device and then stained with RuO_4 vapor for TEM analysis.[43] Aero-spraying was used because this technique helped break up the micellar solution into a fine spray and accelerate the evaporation of the solvent FEMA to avoid possible morphological changes of the aggregates during solvent evaporation. Images a and b in Figure 1 show TEM images of the sprayed and stained aggregates of $F_{66}M_{200}$ and $F_{95}A_{135}$, respectively. Analogous images were also obtained of the cross-linked aggregates (see Figure S3 in the Supporting Information). Because the cross-linked aggregates were unlikely to change their shapes drastically during TEM specimen preparation, this suggested that the sprayed samples retained their original shapes that they exhibited in solution.

The $F_{66}M_{200}$ particle marked by the arrow in Figure 1a had a dark rim and a gray center. The diameter of the marked particle including the rim was 100 ± 15 nm and the thickness of the rim was 5.2 ± 1.8 nm. The other particles in Figure 1a had a composite rim with an average thickness of 22.2 ± 3.1 nm. The

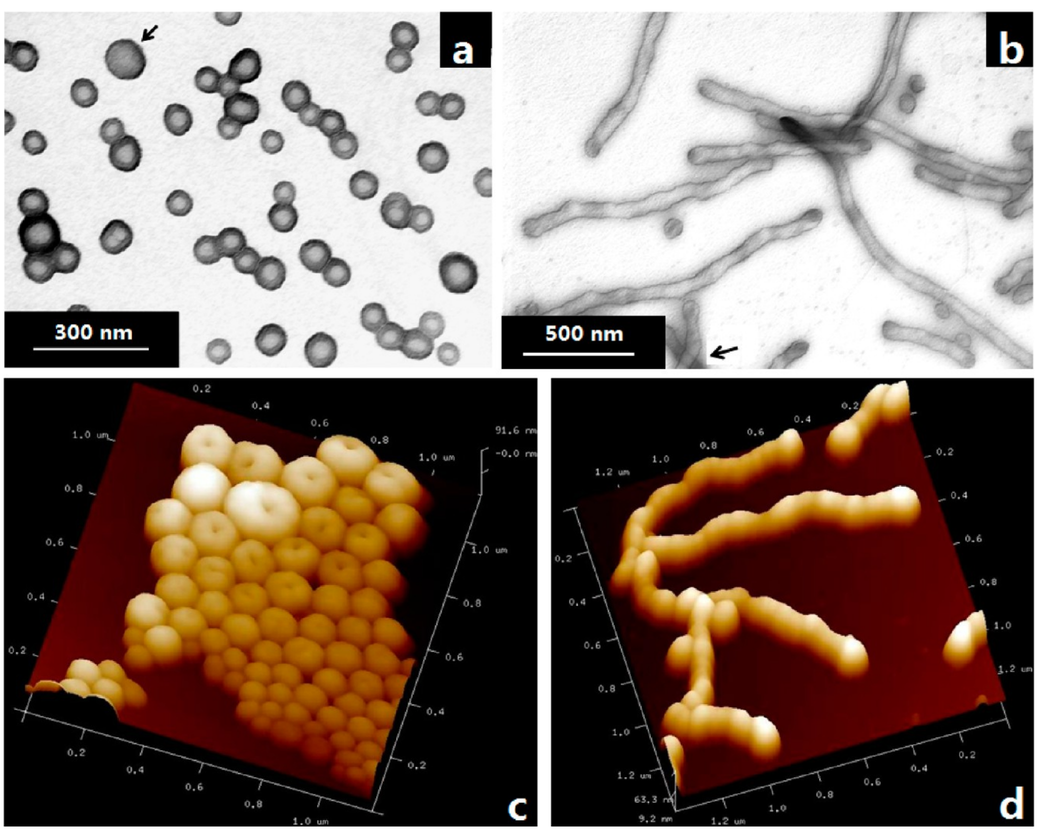

Figure 1. TEM images (top) of (a) vesicular $F_{66}M_{200}$ aggregates and (b) tubular $F_{95}A_{135}$ micelles, which were aero-sprayed from FEMA and stained with RuO_4. Also shown are AFM topography images of the corresponding (c) $F_{66}M_{200}$ and (d) $F_{95}A_{135}$ samples.

dx.doi.org/10.1021/am400058k | ACS Appl. Mater. Interfaces 2013, 5, 2378−2386

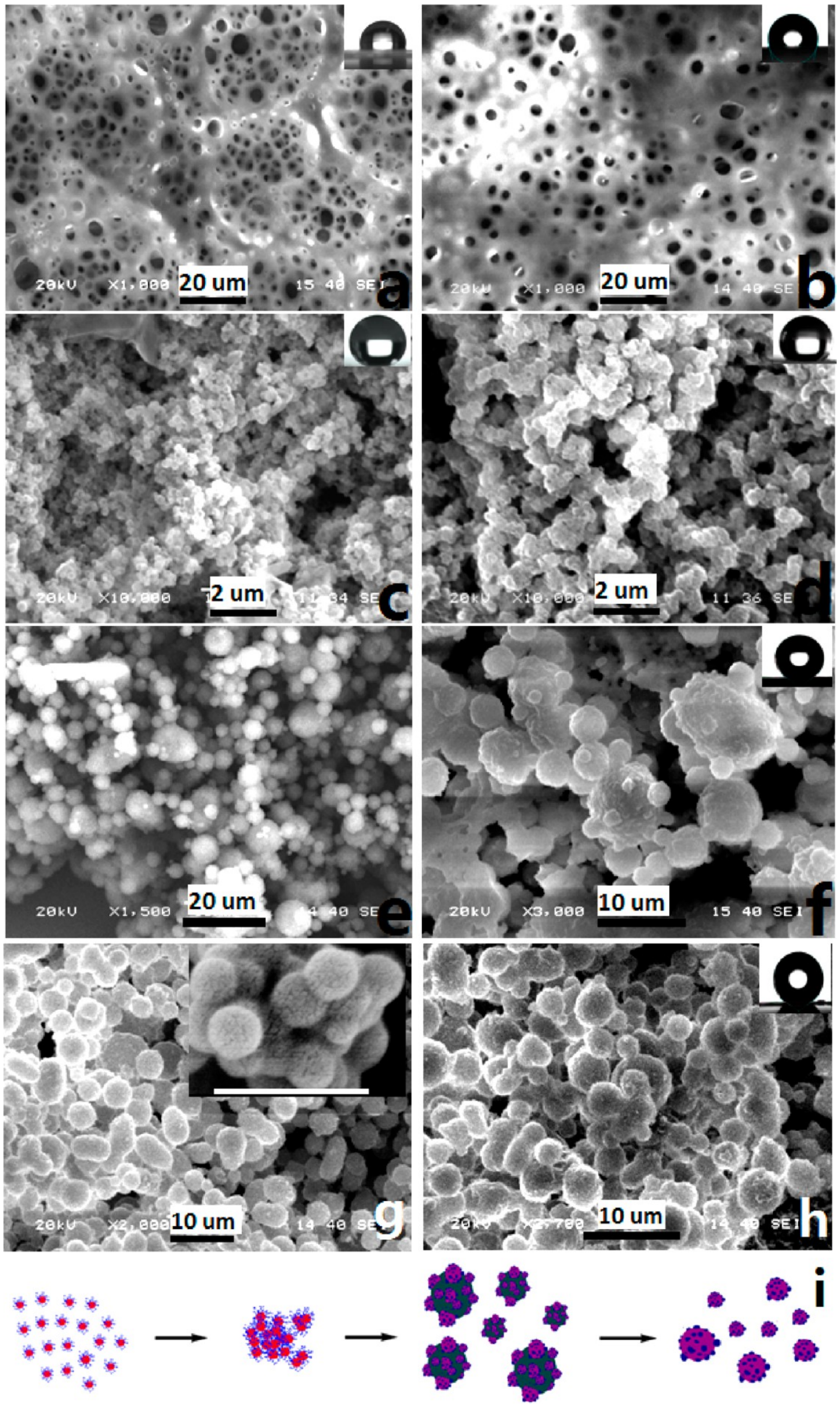

Figure 2. SEM images of films of cross-linked $F_{66}M_{200}$ hollow nanospheres cast from CH_2Cl_2/MeOH at f_{MeOH} = (a)0, (b) 10, (c) 20, (d) 25, (e, f) 30, and (g, h) 50%. (i) Illustrated mechanism for the formation of hierarchical particles. The scale bar in the inset of image g corresponds to 400 nm.

composite rim consisted of a gray layer that was sandwiched between two dark layers, which each had a thickness of ∼5 nm.

We concluded that the marked particle in Figure 1a was a "normal", rather than a collapsed, vesicle based on the following considerations. First, the particle could not be a spherical micelle. If it were a spherical micelle, the center of the particle would have been much darker. Second, the contour length of a fully stretched M_{200} chain would be ∼50 nm, which was far smaller than the average particle diameter of 100 nm. Third, the color variation observed in the TEM images of the particles was consistent with that of a vesicular structure, where the insoluble M shell was selectively stained and appeared darker in the peripheral region while the core appeared lighter. The shell appeared darker at the periphery, because the path length of the TEM electrons was greater in the regions where the shell was in a standing vertical position.

According to Azzam and Eisenberg,[44] the particles with a composite rim were collapsed vesicles. The collapsed vesicles assumed hemispherical or Kippah-like shapes, in which the walls had merged together to form a double-wall. These merged walls would have sandwiched the original F chains that occupied the internal surface of each wall, this F layer appeared as a lighter layer between two dark layers. We do not know the exact reason why these vesicles collapsed so readily. The thinness of the M layer, and thus the flexibility of the wall, was probably a cause for this behavior. This was judged by the fact that most of the cross-linked vesicles are "normal", with a single rim rather than a composite rim due to the improved rigidity of the cross-linked wall belonging to the vesicular aggregates (see Figure S3 in the Supporting Information).

To confirm the vesicular structure, the aggregates were aero-sprayed onto freshly cleaved mica and analyzed via AFM. Figure 1c shows an AFM topography image of a vesicular sample of $F_{66}M_{200}$. Round particles and particles bearing a crater (collapsed particles) coexisted in the sample. Thus, the AFM results unambiguously confirmed the TEM results. While the average diameter of the particles in Figure 1c was 120 ± 30 nm, their height was in the range of 25−35 nm as determined via section−sectional analysis (see Figure S4 in the Supporting Information). This large difference between the average diameter and height was mainly due to the lack of rigidity of the M walls and thus the flattening of the vesicles on mica. The low rigidity of the M wall was also responsible for the collapse of many vesicles.

The diameter of the elongated structures in Figure 1b varied from section to section and the average diameter was 60 ± 5 nm. These structures had a lighter core and a darker rim, suggesting that the structures shown in Figure 1b were tubular rather than cylindrical micelles. We reached this conclusion based on the following considerations: First, the fully stretched length of an A_{135} chain should be 34 nm and it would have been difficult to prepare solid A cylinders with a diameter of 60 ± 5 nm from such short A_{135} chains. Second, one can see the underlying structure when two structures crossed over one another. One of these intersections is marked by an arrow in Figure 1b. The observation of an underlying structure would normally be very difficult if structures of this size were solid, rather than hollow. Third, the backbone of the elongated structures undulated. This undulation was probably due to the nonuniform collapse of nanotubes when the solvent evaporated, as was observed previously among other nanotubes.[45]

This tubular structure of the $F_{95}A_{135}$ aggregates was also consistent with AFM observation. Figure 1d shows a topography image of tubular micelles that had been aero-sprayed onto a mica surface. While the structures were elongated, they were also undulated.

While there have been many reports on the preparation of spherical micelles, cylindrical micelles, and vesicles, reports on self-assembled tubular micelles of block copolymers have been rare.[46] The facile formation of tubular micelles in this case warrants a future study.

The vesicles and tubular micelles were photolyzed with UV light to cross-link the M and A walls.[31] After photolysis treatment had provided the M walls with double bond conversions of ~40%, as determined by UV absorbance analysis at 273 nm,[31] the particles retained their shapes. This structural rigidity was maintained even after the particles had been precipitated from hexane and redispersed into dichloromethane, a good solvent for both F and un-cross-linked M or A chains. Thus, the photolysis helped yield permanent hollow nanospheres and nanotubes.

A control experiment was performed involving the photolysis of FEMA alone in the absence of FM or FA. The monomer did not cross-link under these conditions. This was reasonable, as FEMA did not absorb light at wavelengths exceeding 210 nm.

3.3. Particulate Films of the Hollow $F_{66}M_{200}$ Nanospheres. Particulate films of $F_{66}M_{200}$ hollow spheres were prepared by casting the spheres from CH_2Cl_2/methanol dispersions with different methanol volume fractions f_{MeOH}. Figure 2 shows SEM images of particulate films that were formed by casting $F_{66}M_{200}$ hollow spheres from CH_2Cl_2/methanol dispersions at f_{MeOH} = 0, 10, 20, 25, 30, and 50%. At these solvent compositions the hollow nanospheres remained dispersed and had not precipitated yet. At f_{MeOH} = 0%, perforated films that bore micrometer-sized holes were formed. Despite these holes, the films had rather smooth surfaces. An analogous film was formed at f_{MeOH} = 10%. The film became rougher when f_{MeOH} was increased to 20 and 25%. In these cases, craters and valleys were observed among ridges and hills formed by the fused individual nanospheres (Figure 2c, d) that had average sizes of 120 ± 21 nm. This size was comparable to the TEM diameter of 100 ± 15 nm determined from the vesicles shown in Figure 1a. The small difference could be due to experimental error or the fact that the SEM diameter corresponded to the whole capsules including the outer F layer. Meanwhile, the TEM diameter represented only the regions of the capsule that were bound by the OsO_4-stained M wall.

At f_{MeOH} = 30%, the cross-linked $F_{66}M_{200}$ nanospheres fused into bumpy microspheres with an average diameter of 4 ± 2 μm. At f_{MeOH} = 50%, the size distribution of the bumpy spheres became narrower and the average diameter was 3 ± 1 μm. To gain structural insight into the microspheres formed at f_{MeOH} = 50%, we also performed a field-emission SEM study, and obtained the image shown as the inset in Figure 2g. The inset clearly shows that the microspheres were made of both collapsed and intact hollow nanospheres. The proposed structure of the bumpy microspheres is shown in Figure 2i.

We initially expected the formation of a smooth film from the hollow nanospheres when they were cast from CH_2Cl_2, a selective solvent for the F coronal chains, because the F chains of different particles could interdigitate and mix. The formation of the perforated films of Figure 1a surprised us initially. Our literature search revealed that these perforated films had been formed via a so-called "Breath Figure" process described by Widawski et al.[47] In their system, fast evaporation of carbon disulfide cooled down the surface of a liquid film and induced water condensation and droplet formation. The holes were derived from the spaces originally occupied by the condensed water droplets. Since its discovery, the "Breath Figure" process has been used to create porous polymer films[48−50] and even superhydrophobic polymeric surfaces.[51] Therefore, this phenomenon could have also occurred in our system.

In our case, the casting of hollow nanosphere dispersions from CH_2Cl_2/MeOH with $f_{MeOH} \geq 30\%$ yielded a collection of microspheres with nanometer-sized bumps, probably because of the hierarchical assembly of the hollow nanospheres during solvent evaporation. Methanol is a poor solvent for F and has a boiling point of 65 °C, which is higher than the 40 °C boiling point of CH_2Cl_2. As CH_2Cl_2 evaporated preferentially, the residual solvent became increasingly poor for the hollow nanospheres. This should have induced nanosphere aggregation into microspheres, leaving behind solvent-rich regions that turned into void space after solvent evaporation. The bumps were probably formed at the later stage of the film formation process, when the amounts of the residual solvent and nanospheres decreased. Consequently, the nanosphere mobility also decreased, so that they could no longer assemble to form smooth surface layers.

According to past reports and our understanding of the lotus-leaf effect,[2,3,47−50] the microspheres bearing nanobumps shown in Figure 2g should provide ideal superhydrophobic surfaces. This was verified by the behavior of water and ink droplets on coatings of $F_{66}M_{200}$ hollow nanospheres cast from CH_2Cl_2/MeOH at f_{MeOH} = 50%. If the droplets were applied from a small height and with some velocity onto a coating that was either slightly slanted or leveled, the droplets readily bounced off the substrate. Figure 3 shows photographs of water and ink droplets that were carefully and slowly applied onto films of $F_{66}M_{200}$ hollow nanospheres that were cast from CH_2Cl_2/MeOH at f_{MeOH} = 50%. The droplets had a contact angle of 160° (inset in Figure 2h), and a sliding angle of ~5° (see Figure S5 in the Supporting Information), confirming the superhydrophobicity of the coating.

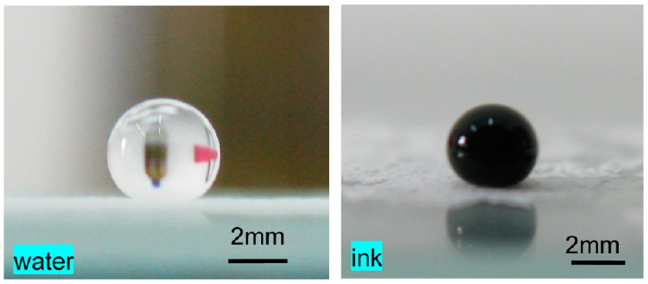

Figure 3. Photographs of water and ink droplets on films of $F_{66}M_{200}$ hollow nanospheres cast from CH_2Cl_2/MeOH at f_{MeOH} = 50%.

Photographs of water droplets that were applied onto nanosphere films cast from dispersions with other f_{MeOH}'s are shown as the insets in Figure 2a−f. The water contact angles were 90°, 102°, 138°, 140° and 153° at f_{MeOH} = 0%, 10%, 20%, 25% and 30%, respectively. Evidently, the microspheres that bore nanobumps were the most effective in rendering superhydrophobicity.

We also performed control experiments and prepared films from noncross-linked copolymer in CH_2Cl_2/MeOH at f_{MeOH} = 0%, 10%, 20%, 25%, and 30%, respectively. The water contact angles of the resulting films were all less than 100°. The methanol content could not be pushed higher because the polymer did not dissolve in CH_2Cl_2/MeOH at f_{MeOH} > 30%. These experiments clearly showed that the cross-linked and noncross-linked copolymers exhibited different film formation properties.

3.4. $F_{95}A_{135}$-Based Nanotube Films. Particulate films were also cast from dispersions of $F_{95}A_{135}$ nanotubes in CH_2Cl_2/MeOH at f_{MeOH} = 0, 40, and 50%. As was the case for films of the $F_{66}M_{200}$ hollow spheres, the $F_{95}A_{135}$ films cast at f_{MeOH} = 0% contained micrometer-sized holes (Figure 4a). While the film appeared rather smooth on the top, the bottoms of the holes appeared to be rough, and consisted of fused nanotubes (Figure 4b). The nanotubes fused into a network that was strewn with interpenetrating or interconnecting holes at f_{MeOH} = 40% (Figure 4c, d).

At f_{MeOH} = 50%, the ridges of the fused nanotube phase became less ribbon-like but began to resemble terraces (Figure 4e, f). Both the ribboned and the terraced network structures of images c and 4e in Figure 4, respectively, appear to belong to the overhanging structure category with many re-entrant surface sites on the lower sides of the networked ribbons or the terraces.[52] Regardless of the appearance of the hierarchically assembled films, images b, d, and f in Figure 4 clearly show that the nanotubes were the basic building units of these films.

The hierarchical structures of the $F_{95}A_{135}$ nanotubes were evidently different from those formed from the hollow nanospheres of $F_{66}M_{200}$. The nanotubes, unlike the hollow spheres, were not able to assemble into bumpy microspheres but instead formed networks of ribbons or terraces. This difference was reasonable because the nanometer structures of the tubes and hollow spheres govern their further assembly behavior.

The water contact angles on nanotube films cast from dispersions with f_{MeOH} = 0, 40, and 50% were measured to be 100, 154, and 160°, respectively. The water sliding angle on the nanotube film cast at f_{MeOH} = 50% was ~3° (see Figure S5 in the Supporting Information). These results demonstrated the superhydrophobicity of the films cast at f_{MeOH} = 50%, and possibly also at f_{MeOH} = 40%.

It should be noted that the water sliding angle of 3° on the nanotube films cast at f_{MeOH} = 50% was smaller than the 5° sliding angle obtained for the hollow sphere film that was also cast at f_{MeOH} = 50%. This suggested that the films formed from nanotubes provided better water repellency than the hollow sphere-based film. Both the hollow spheres and the nanotubes were covered by F chains and thus had the same surface chemical composition. Therefore, these differing wetting properties must have derived from differences in the hierarchical structures of the films formed from the two groups of nanostructures.

4. CONCLUSIONS

Two diblock copolymers $F_{66}M_{200}$ and $F_{95}A_{135}$ consisting of a fluorinated block and a photo-cross-linkable block were synthesized via ATRP and were characterized. In FEMA, a block-selective solvent for the F block, $F_{66}M_{200}$, and $F_{95}A_{135}$ formed vesicles and tubular micelles, respectively. There have been very few reports on diblock copolymer tubular micelles. Their formation from $F_{95}A_{135}$ deserves a further investigation and an understanding of this system may provide a general pathway toward tubular micelles.

Photolyzing these assembled aggregates yielded hollow nanospheres and nanotubes as permanent structures. Casting films from CH_2Cl_2/MeOH dispersions of these particles, where CH_2Cl_2 was a good solvent and MeOH was a poor solvent for the tubes or hollow spheres, yielded films whose morphology changed depending on f_{MeOH}, and the particles used. At f_{MeOH} = 0%, films with micrometer-sized holes but rather flat ridged surfaces were formed. At f_{MeOH} values of 20 and 25%, rough or porous films were formed from $F_{66}M_{200}$ hollow spheres. The ridges consisted of randomly aggregated nanospheres. Meanwhile, at f_{MeOH} ≥ 30%, the $F_{66}M_{200}$ nanospheres underwent hierarchical assembly to yield bumpy microspheres. The cross-linked nanotubes self-assembled into a highly porous network consisting of fibrous ridges at f_{MeOH} = 40%. Interconnected terrace-like structures were obtained from the assembly of the cross-linked nanotubes at f_{MeOH} = 50%. The above results suggest that solution casting of nanoparticles from a mixture of good and poor solvents may provide a general method for preparing rough films. The fine structure of fused particle matrix can be tuned by changing either the solvent mixture

dx.doi.org/10.1021/am400058k | ACS Appl. Mater. Interfaces 2013, 5, 2378−2386

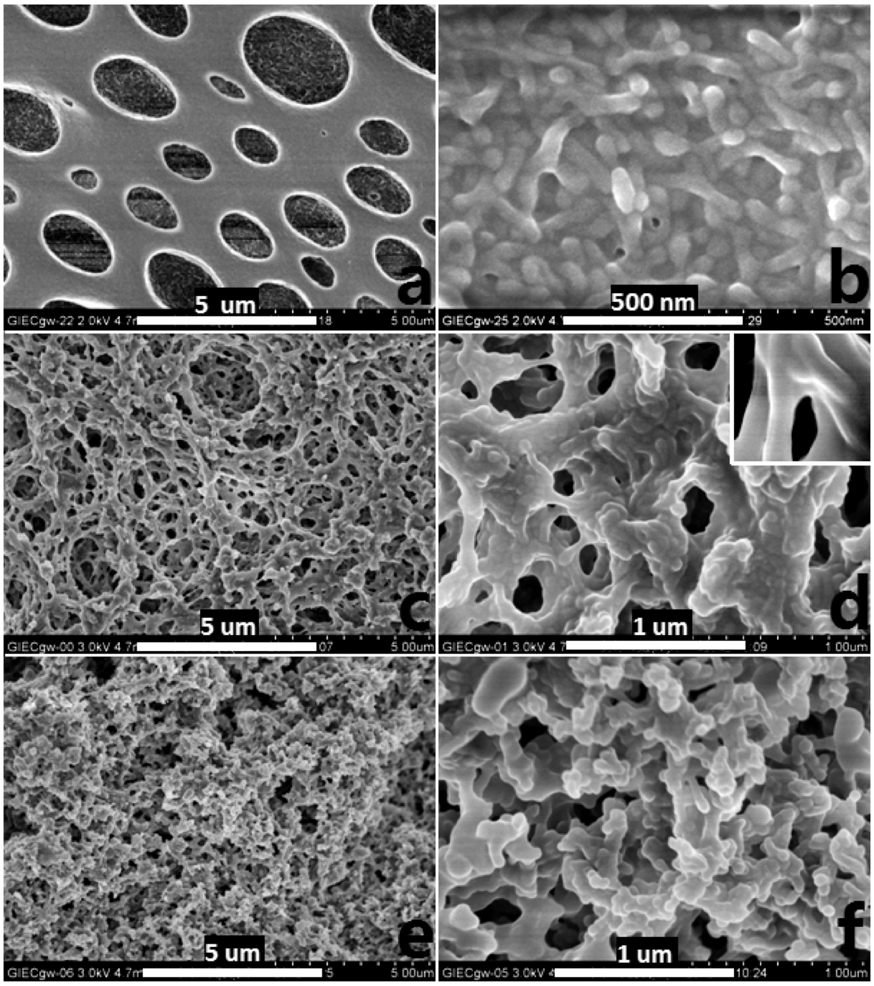

Figure 4. SEM images of $F_{95}A_{135}$ nanotube films cast from CH_2Cl_2/MeOH at f_{MeOH} = (a, b) 0, (c, d) 40, and (e, f) 50%, respectively. The inset in d shows an area with higher magnification.

composition or the structure of the primary assembling particles.

Although films that were hierarchically assembled from either the hollow spheres or the tubes at f_{MeOH} = 50% were superhydrophobic, the water repellency of the films formed from the fused nanotubes was higher, as attested by the lower water sliding angles on the latter films. This result was consistent with the richness of overhanging structures seen in the rough film made from the nanotubes. Overhanging structures will be useful in the preparation of superoelophobic surfaces.

■ ASSOCIATED CONTENT

Supporting Information

TEM images of vesicular FM aggregates and tubular FA micelles before and after cross-linking, AFM height images with sectional-analysis of vesicular FM aggregates and tubular FA micelles, as well as the images of the sliding of a water droplet on the surface. This material is available free of charge via the Internet at http://pubs.acs.org/.

■ AUTHOR INFORMATION

Corresponding Author

*E-mail: hjw@gic.ac.cn. Fax: 86-20-85232307.

Notes

The authors declare no competing financial interest.

■ ACKNOWLEDGMENTS

We thank the National Natural Science Foundation of China (20474068, 51173204), the Outstanding Overseas Chinese Scholars Funds of the Chinese Academy of Sciences, and the Leading Talents Program of Guangdong Province for financial support. We also thank Dr. Ian Wyman from the Chemistry Department of Queen's University (Canada) for English proofing of the paper.

■ REFERENCES

(1) Wang, S.; Jiang, L. *Adv. Mater.* **2007**, *19*, 3423−3424.
(2) Solga, A.; Cerman, Z.; Striffler, B. F.; Spaeth, M.; Barthlott, W. *Bioinspir. Biomim.* **2007**, *2*, S126−S134.
(3) Gao, X. F.; Jiang, L. *Nature* **2004**, *432*, 36−36.
(4) Blossey, R. *Nat. Mater.* **2003**, *2*, 301−306.
(5) Cao, L. L.; Jones, A. K.; Sikka, V. K.; Wu, J. Z.; Gao, D. *Langmuir* **2009**, *25*, 12444−12448.
(6) (a) Liu, K. S.; Jiang, L. *Nanoscale* **2011**, *3*, 825−838. (b) Weng, C. J.; Chang, C. H.; Peng, C. W.; Chen, S. W.; Yeh, J. M.; Hsu, C. L.; Wei, Y. *Chem. Mater.* **2011**, *23*, 2075−2083. (c) Weng, C. J.; Peng, C. W.; Chang, C. H.; Chang, Y. H.; Yeh, J. M. *J. Appl. Polym. Sci.* **2012**, *126*, E48−E55. (d) Yang, T. I.; Peng, C. W.; Lin, Y. L.; Weng, C. J.; Edgington, G.; Mylonakis, A.; Huang, T. C.; Hsu, C. H.; Yeh, J. M.; Wei, Y. *J. Mater. Chem.* **2012**, *22*, 15845−15852.

(7) Nosonovsky, M.; Bhushan, B. *J. Phys. Condens. Mater.* **2008**, *20*, 220510−225033.
(8) Bico, J.; Marzolin, C.; Quere, D. *Europhys. Lett.* **1999**, *47*, 220−226.
(9) Chen, W.; Fadeev, A. Y.; Hsieh, M. C.; Oner, D.; Youngblood, J.; McCarthy, T. J. *Langmuir* **1999**, *15*, 3395−3399.
(10) Park, S. G.; Moon, H. H.; Lee, S. K.; Shim, J.; Yang, S. M. *Langmuir* **2010**, *26*, 1468−1472.
(11) Li, Y. F.; Zhang, J. H.; Zhu, S. J.; Dong, H. P.; Jia, F.; Wang, Z. H.; Tang, Y.; Zhang, L. A.; Zhang, S. Y.; Yang, B. *Langmuir* **2010**, *26*, 9842−9847.
(12) Ling, X. Y.; Phang, I. Y.; Vancso, G. J.; Huskens, J.; Reinhoudt, D. N. *Langmuir* **2009**, *25*, 3260−3263.
(13) Ma, M. L.; Hill, R. M.; Lowery, J. L.; Fridrikh, S. V.; Rutledge, G. C. *Langmuir* **2005**, *21*, 5549−5554.
(14) Qian, T. C.; Li, Y. F.; Wu, Y. Z.; Zheng, B.; Ma, H. W. *Macromolecules* **2008**, *41*, 6641−6645.
(15) Tuberquia, J. C.; Nizamidin, N.; Harl, R. R.; Albert, J.; Hunter, J.; Rogers, B. R.; Jennings, G. K. *J. Am. Chem. Soc.* **2010**, *132*, 5725−5734.
(16) Feng, L.; Song, Y. L.; Zhai, J.; Liu, B. Q.; Xu, J.; Jiang, L.; Zhu, D. B. *Angew. Chem., Int. Ed.* **2003**, *42*, 800−802.
(17) Munoz-Bonilla, A.; Bousquet, A.; Ibarboure, E.; Papon, E.; Labrugere, C.; Rodriguez-Hernandez, J. *Langmuir* **2010**, *26*, 16775−16781.
(18) Lim, J. M.; Yi, G. R.; Moon, J. H.; Heo, C. J.; Yang, S. M. *Langmuir* **2007**, *23*, 7981−7989.
(19) Wang, H. X.; Fang, J.; Cheng, T.; Ding, J.; Qu, L. T.; Dai, L. M.; Wang, X. G.; Lin, T. *Chem. Commun.* **2008**, 877−879.
(20) Ofir, Y.; Samanta, B.; Arumugam, P.; Rotello, V. M. *Adv. Mater.* **2007**, *19*, 4075−4079.
(21) Xiong, D.; Liu, G. J.; Hong, L. Z.; Duncan, E. J. S. *Chem. Mater.* **2011**, *23*, 4357−4366.
(22) Xiong, D. A.; Liu, G. J.; Zhang, J. G.; Duncan, S. *Chem. Mater.* **2011**, *23*, 2810−2820.
(23) Cui, X. J.; Zhong, S. L.; Yan, J.; Wang, C. L.; Zhang, H. T.; Wang, H. Y. *Colloids Surf., A* **2010**, *360*, 41−46.
(24) Sawada, H.; Shikauchi, Y.; Kakehi, H.; Katoh, Y.; Miura, M. *Colloid Polym. Sci.* **2007**, *285*, 499−506.
(25) Visintin, P. M.; Carbonell, R. G.; Schauer, C. K.; DeSimone, J. M. *Langmuir* **2005**, *21*, 4816−4823.
(26) Mugisawa, M.; Sawada, H. *Langmuir* **2008**, *24*, 9215−9218.
(27) Zhang, L. F.; Eisenberg, A. *Science* **1995**, *268*, 1728−1731.
(28) Hayward, R. C.; Pochan, D. J. *Macromolecules* **2010**, *43*, 3577−3584.
(29) Ding, J. F.; Liu, G. J.; Yang, M. L. *Polymer* **1997**, *38*, 5497−5501.
(30) Liu, G. J. In *Block Copolymers in Nanoscience*; Lazzari, M., Liu, G. J., Lecommandoux, S., Eds.; Wiley-VCH: Weinheim, Germany, 2006; p 233.
(31) Tao, J.; Guo, A.; Liu, G. J. *Macromolecules* **1996**, *29*, 1618−1624.
(32) Liu, G. J.; Qiao, L. J.; Guo, A. *Macromolecules* **1996**, *29*, 5508−5510.
(33) Stewart, S.; Liu, G. *Angew. Chem., Int. Ed.* **2000**, *39*, 340−344.
(34) Thurmond, K. B.; Kowalewski, T.; Wooley, K. L. *J. Am. Chem. Soc.* **1996**, *118*, 7239−7240.
(35) Ding, J. F.; Liu, G. J. *Chem. Mater.* **1998**, *10*, 537−542.
(36) Liu, G. J.; Ding, J. F.; Guo, A.; Herfort, M.; BazettJones, D. *Macromolecules* **1997**, *30*, 1851−1853.
(37) Liu, G. J.; Xu, X. Q.; Skupinska, K.; Hu, N. X.; Yao, H. *J. Appl. Polym. Sci.* **1994**, *53*, 1699−1707.
(38) (a) Xie, Q. D.; Fan, G. Q.; Zhao, N.; Guo, X. L.; Xu, J.; Dong, J. Y.; Zhang, L. Y.; Zhang, Y. J.; Han, C. C. *Adv. Mater.* **2004**, *16*, 1830−1833. (b) Zhao, N.; Xie, Q. D.; Weng, L. H.; Wang, S. Q.; Zhang, X. Y.; Xu, J. *Macromolecules* **2005**, *38*, 8996−8999.
(39) (a) Desbief, S.; Grignard, B.; Detrembleur, C.; Rioboo, R.; Vaillant, A.; Seveno, D.; Voue, M.; De Coninck, J.; Jonas, A. M.; Jerome, C.; Damman, P.; Lazzaroni, R. *Langmuir* **2010**, *26*, 2057−2067. (b) Han, J. T.; Xu, X. R.; Cho, K. W. *Langmuir* **2005**, *21*, 6662−6665. (c) Cui, Z.; Ding, J. F.; Scoles, L.; Wang, Q. J.; Chen, Q. M. *Macromol. Chem. Phys.* **2010**, *211*, 1757−1764. (d) Li, H.; Zhao, Y. H.; Yuan, X. Y. *Soft Matter* **2013**, *9*, 1005−1009.
(40) Feng, L.; Hu, J. W.; Liu, Z. L.; Zhao, F. B.; Liu, G. J. *Polymer* **2007**, *48*, 3616−3623.
(41) Beers, K. L.; Boo, S.; Gaynor, S. G.; Matyjaszewski, K. *Macromolecules* **1999**, *32*, 5772−5776.
(42) He, G. P.; Zhang, G. W.; Hu, J. W.; Sun, J. P.; Hu, S. Y.; Li, Y. H.; Liu, F.; Xiao, D. S.; Zou, H. L.; Liu, G. J. *J. Fluorine Chem.* **2011**, *132*, 562−572.
(43) Ding, J. F.; Liu, G. J. *Macromolecules* **1999**, *32*, 8413−8420.
(44) Azzam, T.; Eisenberg, A. *Langmuir* **2010**, *26*, 10513−10523.
(45) Yan, X. H.; Liu, G. J.; Liu, F. T.; Tang, B. Z.; Peng, H.; Pakhomov, A. B.; Wong, C. Y. *Angew. Chem., Int. Ed.* **2001**, *40*, 3593−3596.
(46) Liu, G. J. *Adv. Polym. Sci.* **2008**, *220*, 29−64.
(47) Widawski, G.; Rawiso, M.; Francois, B. *Nature* **1994**, *369*, 387−389.
(48) Ferrari, E.; Fabbri, P.; Pilati, F. *Langmuir* **2011**, *27*, 1874−1881.
(49) Hernandez-Guerrero, M.; Stenzel, M. H. *Polym. Chem.* **2012**, *3*, 563−577.
(50) Escale, P.; Rubatat, L.; Billon, L.; Save, M. *Eur. Polym. J.* **2012**, *48*, 1001−1025.
(51) Yabu, H.; Takebayashi, M.; Tanaka, M.; Shimomura, M. *Langmuir* **2005**, *21*, 3235−3237.
(52) (a) Tuteja, A.; Choi, W.; Ma, M. L.; Mabry, J. M.; Mazzella, S. A.; Rutledge, G. C.; McKinley, G. H.; Cohen, R. E. *Science* **2007**, *318*, 1618−1622. (b) Tuteja, A.; Choi, W. J.; McKinley, G. H.; Cohen, R. E.; Rubner, M. F. *MRS Bull.* **2008**, *33*, 752−758.